Effect of a stabilizing gradient of solute on thermal convection

By GEORGE VERONIS

Geology and Geophysics Department, Yale University, New Haven, Connecticut

A stabilizing gradient of solute inhibits the onset of convection in a fluid which is subjected to an adverse temperature gradient. Furthermore, the onset of instability may occur as an oscillatory motion because of the stabilizing effect of the solute. These results are obtained from linear stability theory which is reviewed briefly in the following paper before finite-amplitude results for two-dimensional flows are considered. It is found that a finite-amplitude instability may occur first for fluids with a Prandtl number somewhat smaller than unity. When the Prandtl number is equal to unity or greater, instability first sets in as an oscillatory motion which subsequently becomes unstable to disturbances which lead to steady, convecting cellular motions with larger heat flux. A solute Rayleigh number, R_s, is defined with the stabilizing solute gradient replacing the destabilizing temperature gradient in the thermal Rayleigh number. When R_s is large compared with the critical Rayleigh number of ordinary Bénard convection, the value of the Rayleigh number at which instability to finite-amplitude steady modes can set in approaches the value of R_s. Hence, asymptotically this type of instability is established when the fluid is marginally stratified. Also, as $R_s \to \infty$ an effective diffusion coefficient, κ_ρ, is defined as the ratio of the vertical density flux to the density gradient evaluated at the boundary and it is found that $\kappa_\rho = -\sqrt{(\kappa\kappa_s)}$ where κ, κ_s are the diffusion coefficients for temperature and solute respectively. A study is made of the oscillatory behaviour of the fluid when the oscillations have finite amplitudes; the periods of the oscillations are found to increase with amplitude. The horizontally averaged density gradients change sign with height in the oscillating flows. Stably stratified fluid exists near the boundaries and unstably stratified fluid occupies the mid-regions for most of the oscillatory cycle. Thus the step-like behaviour of the density field which has been observed experimentally for time-dependent flows is encountered here numerically.

1. Introduction and discussion

A vertical gradient of solute, such as salt, in a layer of fluid can serve to inhibit the onset of convection when the fluid is heated from below. The effect of the solute on the stability of the fluid layer and some effects on finite-amplitude motion for two-dimensional flows have been discussed by Sani (1965) and by Veronis (1965).† This paper extends the study of paper I to give accurate

† We shall refer to this as paper I.

quantitative results for a range of Rayleigh numbers, R, which differ by as much as an order of magnitude from the critical values of linear stability theory. We consider free, perfectly conducting boundaries at top and bottom.

In the earlier paper we found that the presence of a stabilizing gradient of solute inhibits convection and also introduces the possibility of oscillatory motions, a possibility which does not exist for ordinary Bénard convection near the critical Rayleigh number. We also deduced that finite-amplitude instabilities leading to steady motions could exist for values of the Rayleigh number significantly lower than the critical value of linear stability theory. The analysis was based on a Fourier series representation which was minimal in the sense that the first finite-amplitude results could be represented but no attempt was made to determine the quantitative validity of the representation. The present work takes into account a representation sufficiently large to produce quantitatively significant results for the phenomena which are discussed.

After the equations and the proposed method of solution are set forth in the next section, we summarize the linear stability analysis and the results from paper I in §3. In addition some recent results of P. G. Baines on the linear problem are discussed. Baines has pointed out that oscillatory motions with zero frequency can be interpreted as steady motions and that these can exist at values of the Rayleigh number below those derived by assuming steady motions from the outset. If R_s denotes the Rayleigh number defined with the imposed stabilizing gradient of solute instead of the imposed destabilizing gradient of temperature (R_s is called the solute Rayleigh number here) and if $\tau = \kappa_s/\kappa$ denotes the ratio of diffusivities of solute and heat, the assumption of steady modes yields the asymptotic result for the critical Rayleigh number, $R \to R_s/\tau$ as $R_s \to \infty$. For oscillatory modes with vanishing frequency, Baines has deduced the asymptotic result $R \to R_s$. Generally we have $\tau < 1$ so that the latter result yields a smaller critical Rayleigh number for non-oscillatory modes.

Our primary purpose in this paper is to determine the behaviour of the convecting system in the presence of a stabilizing solute gradient. For this purpose we choose the values of the parameters so that the results can be derived economically on a computer. This means that the important case of $\tau = 0.01$ which corresponds to thermal convection with a salt gradient could not be treated but this is offset by the fact that we can deduce the behaviour of the system for a range of R_s which would otherwise be unattainable. In specific calculations we have worked with $\tau = 10^{-\frac{1}{2}}$ and $\tau = 2^{-\frac{1}{2}}$.

If we denote by R_c the value of the critical Rayleigh number in the absence of a solute gradient, we can expect that for $R_s < R_c$ the effect of the solute will be small whereas for $R_s \gg R_c$ the effect will dominate. Hence, since $R_c = \frac{27}{4}\pi^4$, we have calculated results for the range $10^{\frac{3}{2}} \leqslant R_s \leqslant 2 \times 10^4$ in order to include results for both extreme situations.

To study the dependence on Prandtl number, σ, we have derived finite-amplitude solutions for $\sigma = 10$, $\sigma = 1$, $\sigma = 0.1$ for a configuration with $R_s = 10^3$, $\tau = 10^{-\frac{1}{2}}$ and for a range of Rayleigh numbers. Linear stability theory predicts that instability to steady modes will occur at $R = R^c = 3820$ for all three cases. Oscillatory modes occur at the values of $R = R^o$ listed under the corresponding

values of σ at the top of table 1. We see that for $\sigma = 0\cdot1$ linear theory predicts that steady motions occur first but that for $\sigma = 1$ and $\sigma = 10$ instability manifests itself in the form of oscillatory motions.

The finite-amplitude calculations confirm that infinitesimal oscillatory motions do indeed occur first for $\sigma = 10$ and $\sigma = 1$. For the case with $\sigma = 0\cdot1$ the first instability which can occur is a finite-amplitude instability. This is evident from table 1 (fifth column), where we note that at $R = 1900$ no convection occurs (the Nusselt number, Nu, equals one) whereas, at $R = 2000$, $Nu = 1\cdot844$, which implies well-developed convection. For the cases with $\sigma = 1$ and $\sigma = 10$ well-developed steady convective motions also exist at $R = 2000$ although, as we noted earlier, an oscillatory motion is established first at the value of the Rayleigh number predicted by linear theory.

With the method of paper I a minimal representation yields a finite-amplitude instability at $R = R^f = 1773$. When we increase the representation to give quantitative results valid to within 1 %, we find that R^f is increased to a value lying between 1900 and 2000. This type of adjustment was also encountered for the case of a rotating fluid (Veronis 1968).

Table 1 also shows that as R is increased to a value much larger than R_s the value of Nu approaches that derived in the absence of a solute. This simply means that, when the destabilizing gradient exceeds the stable gradient sufficiently, the system convects and mixes the solute. The fact that the latter has a small diffusion coefficient implies that the solute cannot adjust back to the inhibiting linear distribution that it has with pure conduction and its effect is correspondingly less.

Computations were carried out for the cases $\sigma = 1, \tau = 10^{-\frac{1}{2}}$ and $\sigma = 1, \tau = 2^{-\frac{1}{2}}$ for values of R_s up to 2×10^4. It was found that finite-amplitude instability leading to steady motions was established at values of R which approached the values of R_s as the latter increased. Turner (1968) has observed the same relationship between R and R_s as the condition which determines the depth of penetration of time-evolving convection cells generated by heating a stably stratified fluid from below. Since the ratio R/R_s corresponds to the ratio of the destabilizing to stabilizing gradients imposed on the system, the conclusion is that finite-amplitude instability takes place asymptotically when the system is marginally gravitationally unstable. The value of the Nusselt number corresponding to the established steady motions increases as R_s increases. Both of these results are intuitively plausible.

Since the fluid is stratified by temperature and solute, diffusion and convection lead to vertical fluxes of heat and solute. These two quantities can be combined to yield a density flux through the fluid. For these steady-state motions one can also calculate the horizontally averaged density gradient at the upper and lower boundaries. Dividing the flux by the gradient thus yields an effective density diffusion coefficient, κ_ρ.† This coefficient will generally be a function of

† Although one does not ordinarily associate a diffusion coefficient with density because the mass velocity is defined to account for all of the flux of density, for multiple-component systems with different diffusion coefficients it may be meaningful to define such a diffusion coefficient for density.

the various parameters of the problem. For example, for given σ and τ the value of κ_p will depend on the values of R and R_s. However, as R/R_s approaches unity we find that κ_p approaches a fixed value independent of the individual values of R and R_s but dependent only on their ratio. The limit, $R/R_s = 1$, is an interesting one because it corresponds to the situation where the *net* imposed density difference is zero, since the effects of temperature and salinity on density just compensate. As we pointed out earlier, as R_s becomes larger, finite-amplitude steady motions first occur for $R \to R_s$ so that the derived effective coefficient of diffusion at $R/R_s = 1$ is appropriate to the situation where finite-amplitude steady motions are first established. When $\tau = 10^{-\frac{1}{2}}$ and $\tau = 2^{-\frac{1}{2}}$ we find in this limit that κ_p tends to $-\sqrt{(\kappa\kappa_s)}$, i.e. that the diffusion coefficient for density is the negative of the square root of the product of the diffusivities of solute and temperature. A heuristic argument by Dr Claes Rooth gives the same result and is also outlined in §4.

Figures 2 and 3 contain spatial descriptions of the field variables for a typical steady-state flow. The horizontally averaged density distribution shown in figure 3c is a composition of the temperature and salinity distributions and reflects the expected convective distortion of the linear conductive profile. The density has a sharper gradient near the boundaries and a relatively uniform value in the mid-regions of the layer.

An analysis of the mean density profile for the finite-amplitude oscillatory flow which exists for a Rayleigh number in the range $R^o < R < R^f$ shows that the horizontally averaged vertical density gradient at the boundary can be either positive or negative even though the net imposed density difference is positive. During the oscillatory cycle the flux of density is always positive downward; so that, during part of the cycle, the density flux is up the density gradient and, during the remainder of the cycle, the density flux is down the density gradient. Hence, κ_p as defined above achieves both positive and negative values at different times under the same external conditions.

Figure 5 contains a time sequence of the mean density profiles over a cycle. The density gradient is gravitationally stable near the boundaries and unstable in the interior over most of the cycle. In view of the fact that the steady-state distributions show mean density gradients which are predominantly unstable gravitationally, this stable structure near the boundary marks a significant difference for the oscillatory flows. Heat and solute are still being transported upward in the oscillatory flow as can be seen in the plots of heat and solute flux in figure 4. However, these fluxes are not in phase and the composition leading to the density flux is out of phase with both the heat and solute fluxes and the net result is a negative vertical density gradient near the boundaries. Hence the time-dependent flow exhibits a step-like structure with positive and negative density gradients. This type of alternate structure has been observed experimentally by Turner & Stommel (1964) and by Turner (1965, 1968) in laboratory experiments of transient flows and is also characteristic of vertical density profiles in nature. The physical conditions under which the observations have been made differ from those set forth here but they are qualitatively similar in some cases. Because prescribed conditions in both nature and in the laboratory experiments

to date lead to transient flows of large amplitude, the present analysis cannot be directly applied. It seems likely that a description of the observed flows can be put together from the two processes discussed here. The transient behaviour is due to the different diffusivities and the resulting phase differences of the individual fields. However, the large amplitudes of the observed flows must involve transports of heat and solute characteristic of the steady-state system.

We remark finally that the period of oscillation associated with the transient flows is shown to be increased by finite-amplitude effects. This result is based on four calculations and is summarized in table 3.

2. Formulation of the problem

A layer of fluid of depth d is subjected to uniform heating from below and uniform cooling from above. Thus the temperatures are given by $T = T_m$ at $z = 0$ and $T = T_m - \Delta T$ at $z = d$. The corresponding values of the solute are $S = S_m$ at $z = 0$ and $S = S_m - \Delta S$ at $z = d$. It is convenient in the following analysis to break up the temperature and solute into two parts, (i) the linear part given above and (ii) the part due to convective redistribution. Thus

$$T_{\text{total}} = T_m - \Delta T \frac{z}{d} + T(x, y, z, t), \quad S_{\text{total}} = S_m - \Delta S \frac{z}{d} + S(x, y, z, t). \quad (2.1)$$

The boundaries are taken to be dynamically free and are also perfect conductors of heat and of the solute. Furthermore, we shall restrict our attention to two-dimensional motions; i.e. quantities are assumed to be independent of the horizontal co-ordinate, y.

The Boussinesq equations of motion which we shall use in the analysis are composed of the equations for the conservation of momentum,

$$\frac{\partial}{\partial t} \mathbf{v} + \mathbf{v} \cdot \nabla \mathbf{v} = -\frac{1}{\rho_m} \nabla p + g(\alpha T - \beta S) \mathbf{k} + \nu \nabla^2 \mathbf{v}, \quad (2.2)$$

the conservation of mass,

$$\frac{\partial u}{\partial x} + \frac{\partial w}{\partial z} = 0, \quad (2.3)$$

the conservation of heat,

$$\frac{\partial T}{\partial t} + \mathbf{v} \cdot \nabla T - w \frac{\Delta T}{d} = \kappa \nabla^2 T, \quad (2.4)$$

and the conservation of solute,

$$\frac{\partial S}{\partial t} + \mathbf{v} \cdot \nabla S - w \frac{\Delta S}{d} = \kappa_s \nabla^2 S, \quad (2.5)$$

where the linearized equation of state

$$\rho = \rho_m (1 - \alpha T + \beta S)$$

has been used in the body force term in (2.2). The unit vertical vector is denoted by $\mathbf{k}$; κ and κ_s are the kinematic diffusivity coefficients of heat and solute

respectively; ρ_m is the mean density of the system; and ν is the kinematic viscosity. The quantities α and β are given by

$$\alpha = -\left(\frac{1}{\rho}\frac{\partial p}{\partial T}\right)_{S,p}, \quad \beta = \left(\frac{1}{\rho}\frac{\partial \rho}{\partial S}\right)_{T,p},$$

and g is gravitational acceleration. The temperature, T, and solute, S, are the deviations from the linear form defined in (2.1). The vector $\mathbf{v} = (u, w)$ is the velocity.

A convenient non-dimensionalization is $\mathbf{v} = \mathbf{v}'\kappa/d$, $t = t'd^2/\kappa$, $(x,z) = d(x',z')$, $T = T'\Delta T$, $S = S'\Delta S$, $p' = pd^2/\rho_m \nu\kappa$. We shall substitute these non-dimensional forms and drop the primes with the understanding that all variables are now non-dimensional. Furthermore, we introduce a streamfunction defined by

$$u = \partial\psi/\partial z, \quad w = -\partial\psi/\partial x \qquad (2.6)$$

and upon eliminating p by cross-differentiating (2.2) we derive the vorticity equation

$$\left(\frac{1}{\sigma}\frac{\partial}{\partial t} - \nabla^2\right)\nabla^2\psi = -R\frac{\partial T}{\partial x} + R_s\frac{\partial S}{\partial x} + \frac{1}{\sigma}J(\psi, \nabla^2\psi). \qquad (2.7)$$

The equations for T and S become

$$\left(\frac{\partial}{\partial t} - \nabla^2\right)T + \frac{\partial\psi}{\partial x} = J(\psi, T), \qquad (2.8)$$

$$\left(\frac{\partial}{\partial t} - \tau\nabla^2\right)S + \frac{\partial\psi}{\partial x} = J(\psi, S), \qquad (2.9)$$

where the Jacobian, J, is defined as

$$J(f, g) = \frac{\partial f}{\partial x}\frac{\partial g}{\partial y} - \frac{\partial f}{\partial y}\frac{\partial g}{\partial x}.$$

The following non-dimensional parameters appear:

$$\left.\begin{array}{lll}\text{ratio of diffusivities:} & \tau = \kappa_s/\kappa, \\ \text{Prandtl number:} & \sigma = \nu/\kappa, \\ \text{Rayleigh number:} & R = g\alpha\Delta Td^3/\nu\kappa, \\ \text{Solute Rayleigh number:} & R_s = g\beta\Delta Sd^3/\nu\kappa.\end{array}\right\} \qquad (2.10)$$

Note that R_s is defined with κ rather than κ_s in the denominator. The boundary conditions are

$$\psi = \frac{\partial^2\psi}{\partial z^2} = T = S = 0 \quad \text{at} \quad z = 0, 1. \qquad (2.11)$$

We shall solve the non-linear problem given by (2.7), (2.8), (2.9) and (2.11) by substituting Fourier series in x and z for ψ, S and T and evaluating the coefficients of a finite number of terms. Thus let

$$\left.\begin{array}{l}\psi = \sum\limits_{n=1}^{N}\sum\limits_{m=1}^{M} a_{mn}\sin m\pi\alpha x\sin n\pi z, \\[2mm] T = \sum\limits_{n=1}^{N}\sum\limits_{m=0}^{M} b_{mn}\cos m\pi\alpha x\sin n\pi z, \\[2mm] S = \sum\limits_{n=1}^{N}\sum\limits_{m=0}^{M} c_{mn}\cos m\pi\alpha x\sin n\pi z,\end{array}\right\} \qquad (2.12)$$

where the a_{mn}, b_{mn}, c_{mn} are generally functions of time, and where M and N are integers which determine the size of the representation. These functional forms satisfy the boundary conditions (2.11). The quantity α in (2.12) is the horizontal wave-number of the basic cell; i.e. the (dimensional) horizontal width of a cell is given by d/α. Throughout the calculations $\alpha^2 = \frac{1}{2}$, the value given by linear stability theory. The coefficients a_{mn}, b_{mn} and c_{mn} are determined by the following equations, which are derived by substituting (2.12) into (2.7), (2.8) and (2.9):

$$\dot{a}_{pq} = -\sigma\pi^2(p^2\alpha^2+q^2)a_{pq} - \frac{\sigma R\alpha p}{\pi(p^2\alpha^2+q^2)}b_{pq} + \frac{\sigma R_s\alpha p}{\pi(p^2\alpha^2+q^2)}c_{pq}$$

$$+ \frac{\pi^2\alpha}{4(p^2\alpha^2+q^2)}\left\{\sum_{m=1}^{p-1}\sum_{n=1}^{q-1}(mq-np)[(p-m)^2\alpha^2+(q-n)^2]a_{mn}a_{p-m,q-n}\right.$$

$$+ \sum_{m=p+1}^{M}\sum_{n=q+1}^{N}(mq-np)[(p-m)^2\alpha^2+(q-n)^2-(m^2\alpha^2+n^2)]a_{m-p,n-q}a_{mn}$$

$$+ \sum_{m=p+1}^{M}\sum_{n=1}^{q-1}[p(n-q)+mq][m^2\alpha^2+(q-n)^2]a_{m-p,n}a_{m,q-n}$$

$$+ \sum_{m=p+1}^{M}\sum_{n=q+1}^{N}[q(m-p)+np][(m-p)^2\alpha^2+n^2-m^2\alpha^2-(n-q)^2]a_{m,n-q}a_{m-p,n}$$

$$+ \sum_{m=p+1}^{M}\sum_{n=1}^{q-1}(nq-mp)[(m-p)^2\alpha^2+(p-n)^2]a_{mn}a_{m-p,q-n}$$

$$+ \sum_{m=1}^{p-1}\sum_{n=q+1}^{N}[p(q-n)-mq][(p-m)^2\alpha^2+n^2]a_{m,n-q}a_{p-m,n}$$

$$+ \sum_{m=1}^{p-1}\sum_{n=q+1}^{N}(np-mq)[(p-m)^2\alpha^2+(n-q)^2]a_{mn}a_{p-m,n-q}\right\}, \tag{2.13}$$

$$\dot{b}_{pq} = -\pi^2(p^2\alpha^2+q^2)b_{pq} - \pi\alpha p a_{pq} + (1-\tfrac{1}{2}\delta_{p0})\tfrac{1}{4}\pi^2\alpha$$

$$\times\left\{\sum_{m=0}^{p-1}\sum_{n=1}^{q-1}(np-mq)a_{p-m,q-n}b_{mn} + \sum_{m=p}^{M}\sum_{n=q+1}^{N}(np-mq)a_{mn}b_{m-p,n-q}\right.$$

$$+ \sum_{m=p+1}^{M}\sum_{n=q+1}^{N}[p(q-n)-mq]a_{m-p,n}b_{m,n-q} + \sum_{m=p}^{M}\sum_{n=q+1}^{N}[p(q-n)-mq]a_{m,n-q}b_{m-p,n}$$

$$+ \sum_{m=p+1}^{M}\sum_{n=q+1}^{N}(np-mq)a_{m-p,n-q}b_{mn} + \sum_{m=0}^{p-1}\sum_{n=q+1}^{N}[p(n-q)+mq]a_{p-m,n}b_{m,n-q}$$

$$+ \sum_{m=0}^{p-1}\sum_{n=q+1}^{N}(mq-np)a_{p-m,n-q}b_{mn} + \sum_{m=p}^{M}\sum_{n=1}^{q-1}[q(m-p)+np]a_{m,q-n}b_{m-p,n}$$

$$+ \sum_{m=p+1}^{M}\sum_{n=1}^{q-1}(mq-np)a_{m-p,q-n}b_{mn}\right\}. \tag{2.14}$$

where p and q range from 0 to M and 1 to N respectively and δ_{ij} is the Kronecker delta. The overdot on the left-hand side of each equation denotes a time derivative. An equation similar to (2.14) gives $\dot{c}_{pq}$ if b_{pq} is replaced by c_{pq} and τ multiplies the first term on the right.

The numerical procedure is described elsewhere (Veronis 1966, 1968) and will not be discussed here. It suffices to note that we choose a maximum number of modes, K, and calculate all components and all interactions such that

$$M + N \leqslant K.$$

Systems with $K = 4, 6, 8$ and 10 were treated. The accuracy of the representation is mentioned in connexion with the different results in §4.

3. Stability analysis

The linear stability problem is obtained when the Jacobian terms in (2.7) to (2.9) are neglected. It has been solved in I and also by Sani (1965), so that here we simply summarize the results. Substituting solution forms

$$\psi \sim e^{pt} \sin \pi \alpha x \sin \pi z; \quad T, s \sim e^{pt} \cos \pi \alpha x \sin \pi z \tag{3.1}$$

into the above linearized equations reduces the problem to the solution of the characteristic equation

$$p^3 + (\sigma + \tau + 1) k^2 p^2 + \left[(\tau + \sigma \tau + \sigma) k^4 - (R - R_s) \frac{\sigma \pi^2 \alpha^2}{k^2} \right] p$$
$$+ \sigma \tau k^2 + (R_s - \tau R) \sigma \pi^2 \alpha^2 = 0, \tag{3.2}$$

where $k^2 = \pi^2(\alpha^2 + 1)$. In the above $p = p_r + ip_i$ is a complex number whose real part, p_r, respresents the growth rate and whose imaginary part, ip_i, contains the time-oscillatory behaviour. The quantity α is the horizontal wave-number corresponding to the cellular solutions (3.1).

If σ, τ and R_s are taken as given and $p_r = 0$, then (3.2) represents the relation between the frequency parameter, p_i, the wave-number, α, and the Rayleigh number R. For this marginally stable state two types of solution are possible. For $p_i \equiv 0$ steady convective modes exist when

$$R = R^c \equiv R_s/\tau + k^6/\pi^2 \alpha^2. \tag{3.3}$$

For arbitrary (real) values of p_i, overstable modes exist when

$$R = R^o \equiv \frac{\sigma + \tau}{1 + \sigma} R_s + \frac{(\sigma + 1 + \tau)(\tau/\sigma + \tau + 1) - \tau}{\sigma + 1} k^6/\pi^2 \alpha^2. \tag{3.4}$$

The corresponding value of p_i is given by

$$p_i^2 = \sigma \left(\frac{\tau}{\sigma} + \tau + 1 \right) k^4 - \sigma (R - R_s) \frac{\pi^2 \alpha^2}{k^2}. \tag{3.5}$$

Both R^c and R^o have minimum values when $\alpha^2 = \frac{1}{2}$. As $R_s \to \infty$, the asymptotic behaviours for R^c, R^o and p_i^2 are

$$R^c \to R_s/\tau, \quad R^o \to \frac{\sigma + \tau}{1 + \sigma} R_s, \quad p_i^2 \to \frac{\sigma}{3(1 + \sigma)} R_s. \tag{3.6}$$

These asymptotic results show that, for small values of τ or large values of σ, $R^o/R^c \to \tau$. If the solute is salt, for example, $R^o/R^c \to 0 \cdot 01$.

Although the above results are formally correct, P. G. Baines of Cambridge University has pointed out to me that an extension of the analysis of the stability problem leads to additional, pertinent results for the convective modes. His point is that, if one takes the limit $p_i \to 0$, then the corresponding set of oscillatory modes with zero frequency can be interpreted as convective modes. These occur with $p_r > 0$, i.e. as growing modes, and in some cases the corresponding value of R is less than R^c.
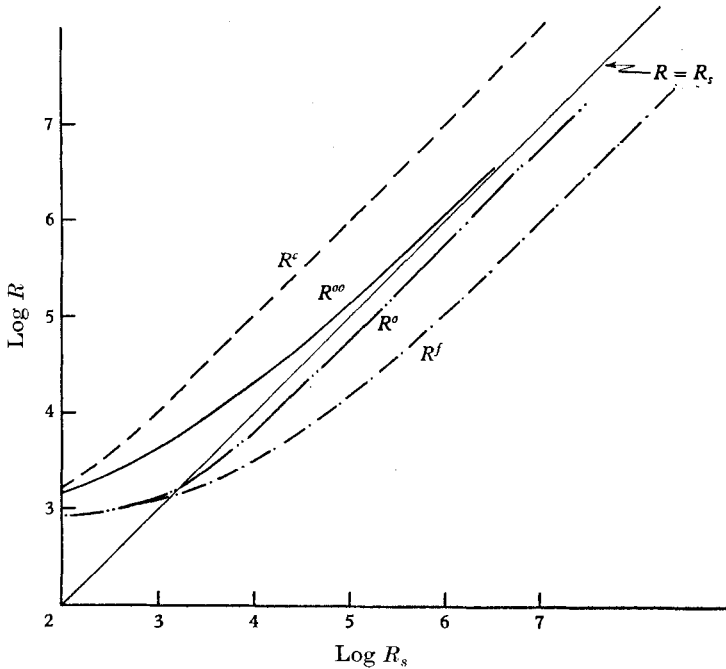
FIGURE 1*a*. Values of R^c, R^o, R^{oo}, and R^f (the latter obtained with $K = 2$) are plotted as functions of R_s for the case $\tau = 10^{-2}$, $\sigma = 10$. The curve for R^{oo} approaches the line $R = R_s$ as R_s becomes large.

Following Baines's procedure we write (3.2) as

$$y^3 + (\sigma + \tau + 1)y^2 + (\tau + \sigma\tau + \sigma - R' + R'_s)y + \sigma\tau + R'_s - \tau R' = 0, \qquad (3.7)$$

where $y = p/k^2$, $R' = R\sigma\pi^2\alpha^2/k^6$, $R'_s = R_s\sigma\pi^2\alpha^2/k^6$. In general, y has three roots, with two of them being complex conjugates and corresponding to oscillatory modes which may grow or decay. The limit of zero frequency is given by the vanishing of the discriminant of (3.7), i.e. by

$$[\tau + \sigma\tau + \sigma - R' + R'_s - \tfrac{1}{3}(\sigma + \tau + 1)^2]^3 + \tfrac{3}{4}[\tfrac{2}{9}(\sigma + \tau + 1)^3$$

$$- (\sigma + \tau + 1)(\tau + \sigma\tau + \sigma - R' + R'_s) + 3(\sigma\tau + R'_s - \tau R')]^2 = 0. \quad (3.8)$$

This is a cubic equation for R' and can readily be solved for different values of σ, τ and R_s. The corresponding value of $R = R'k^6/\sigma\pi^2\alpha^2$ (this will be denoted by R^{oo} for the case where the frequency of the oscillation vanishes) achieves its minimum for $\alpha^2 = \frac{1}{2}$. Asymptotically it is clear that $R' \to R'_s$ or $R \to R_s$ as $R_s \to \infty$. Hence, if steady convection is interpreted as the limiting case of R^o as $p_i \to 0$, the

value of R for which steady motions can first occur is lower than predicted by steady theory and as $R_s \to \infty$ steady motions can take place as soon as the fluid is gravitationally unstable.†
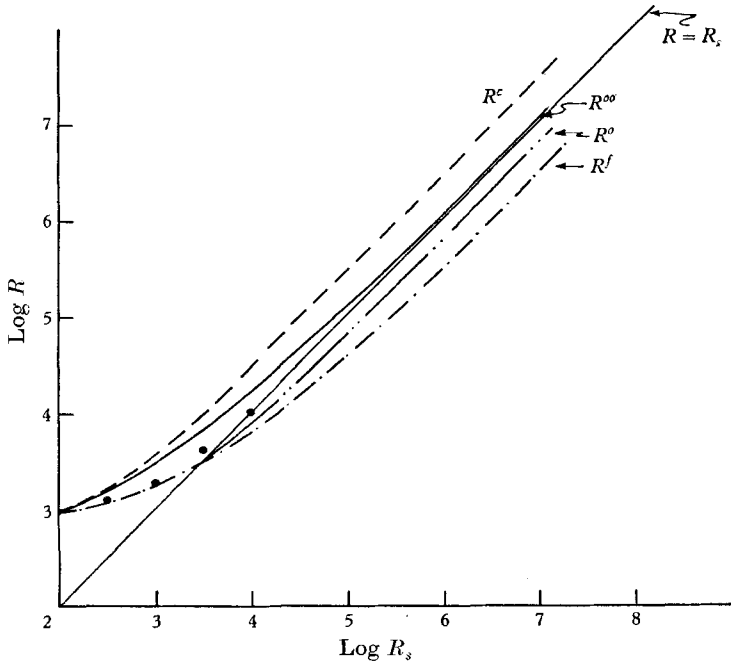
FIGURE 1b. Values of R^c, R^o, R^{oo} and R^f (the latter obtained with $K = 2$) are plotted as functions of R_s for the case $\tau = 10^{-\frac{1}{2}}$, $\sigma = 1$. R^{oo} approaches the line $R = R_s$ asymptotically. Also shown by black dots are the values of R^f obtained with $K = 10$.

Finally, second-order theory based on an analysis with $K = 2$ predicts that finite-amplitude steady motions occur at values of R (denoted by R^f) considerably lower than those values predicted by linear theory. The analysis in I shows that these motions occur for

$$R^f = \left[(\tau R_s)^{\frac{1}{2}} + \left((1 - \tau^2) \frac{\pi^4 (1 + \alpha^2)^3}{\alpha^2} \right)^{\frac{1}{2}} \right]^2 \tag{3.9}$$

and, since R^f achieves a minimum at $\alpha^2 = \frac{1}{2}$, for

$$R^f = [(\tau R_s)^{\frac{1}{2}} + ((1 - \tau^2) \tfrac{27}{4} \pi^4)^{\frac{1}{2}}]^2. \tag{3.10}$$

Asymptotically $R^f \to \tau R_s$ as $R_s \to \infty$. One of the purposes of the present study is to determine the change in R^f as K is increased.

In figure 1 the above results are summarized for $\tau = 10^{-2}$, $\sigma = 10$ (approximately the values for salt water) and $\tau = 10^{-\frac{1}{2}}$, $\sigma = 1$.

† The fact remains, of course, that $R^{oo} > R^o$ so that oscillatory motions will occur first. The value R^{oo} stands as a correction to R^c and, although the linear analysis still predicts instability to oscillatory modes, the above result may be useful for interpreting some of the finite-amplitude results.

4. Finite-amplitude, steady flows

The principal integral results which are described below are the values of the Nusselt number, Nu, and the solute Nusselt number, Nu^s, as functions of R, R_s, τ and σ. The Nusselt number is defined as the ratio of the vertical heat flux, H, to the conductive vertical heat flux. In the steady state the vertical kinematic heat flux is independent of the vertical co-ordinate, z, and can be evaluated as

$$H = \kappa \left\langle \frac{\partial}{\partial z} T_{\text{total}} \right\rangle_{z=0}, \tag{4.1}$$

where the angular brackets correspond to a horizontal average. With the definition of T_{total} from (2.1), (4.1) can be written

$$H = \kappa \frac{\Delta T}{d} - \kappa \frac{\Delta T}{d} \sum_{n=1}^{N} n\pi b_{0n} \tag{4.2}$$

and the Nusselt number is

$$Nu = \frac{H}{\kappa \Delta T/d} = 1 - \pi \sum_{n=1}^{N} n b_{0n}. \tag{4.3}$$

Similarly
$$Nu^s = 1 - \pi \sum_{n=1}^{N} n c_{0n}. \tag{4.4}$$

Choice of values of external parameters

Our purpose is to determine the effect of the stabilizing gradient of the solute on the destabilizing effect of the adverse temperature gradient. The results on stability given in the foregoing section clearly outline the magnitude of the effects of R_s. Thus when R_s is sufficiently small (much less than $R_c = \frac{27}{4}\pi^4$, the critical Rayleigh number for ordinary Bénard convection with no solute present) the effect of the solute is to modify the results for ordinary convection by only a small amount. As R_s is increased to the order of R_c, the values of R at which the various types of instability can first occur also increase and as R_s becomes very large the values of R^c, R^o, R^f and R^{oo} approach asymptotic values. The exact behaviour of the system as a function of R_s depends on τ, the ratio of the diffusivities, as well as on the Prandtl number, σ. The dependency on σ does not appear to be very strong so that only a few results for σ different from unity are reported.

The method of solution which is employed here gives accurate results for only limited ranges of the external parameters. In particular, we note that, when finite-amplitude convection occurs, the temperature and solute profiles are no longer linear in z and, in fact, become quite distorted. The heat flux is given by (4.1) and a similar expression obtains for the solute flux. Hence, the relative magnitudes of heat flux and solute flux are determined in part by the ratio $\tau = \kappa_s/\kappa$. The more that τ differs from unity, the larger the difference in boundary gradients of S and T. Hence, as τ becomes smaller, more terms are needed in the expansion to describe the spatial distribution of the solute.

We restrict our calculations to the cases $\tau = 2^{-\frac{1}{2}}$ and $\tau = 10^{-\frac{1}{2}}$ and determine the dependence of the results on τ by what can be extracted from a comparison of the results for these two values. In order to deduce the behaviour of the system

on R_s we have carried out calculations in the range $10^{\frac{3}{2}} \leqslant R_s \leqslant 2 \times 10^4$ so that we treat flows where $R_s < R_c$ and also $R_s \gg R_c$. Thus we consider systems for which the stabilizing gradient is mild and others for which the stabilizing gradient is dominating.

Heat flux and solute flux

In table 1 the values of Nu and Nu^s for several values of R for the case $\tau = 10^{-\frac{1}{2}}$, $R_s = 10^3$ are tabulated. The first three columns give the results obtained with $K = 6, 8, 10$ for $\sigma = 1$. The degree to which the values of Nu and Nu^s agree for successively larger values of K reveals the accuracy of the representation. Thus

R	$\sigma = 1\cdot0$ $R^o = 1{,}797$ $K = 6$	$K = 8$	$K = 10$	$\sigma = 10$ $R^o = 1{,}831$ $K = 10$	$\sigma = 0\cdot1$ $R^o = 3{,}981$ $K = 10$	$\sigma = 1\cdot0$ $R_s = 0$ $K = 8$
1,797	1·0	1·0	1·0	1·0	1·0	—
	1·0	1·0	1·0	1·0	1·0	—
1,900	Osc.	Osc.	Osc.	Osc.	1·0	—
					1·0	—
2,000	3·314	3·307	3·307	3·279	3·393	—
	1·792	1·787	1·787	1·769	1·844	2·696
2,500	4·425	4·450	4·451	4·460	4·450	—
	2·513	2·505	2·505	2·506	2·507	2·981
5,000	5·919	6·372	6·490	6·436	6·544	—
	3·731	3·714	3·709	3·681	3·736	3·923
10,000	—	7·756	8·360	—	—	—
	—	4·961	4·965	—	—	5·064

TABLE 1. Nu^s and Nu vs. R and σ. The values of Nu^s and Nu (with Nu^s the upper value in each pair) for $\tau = 10^{-\frac{1}{2}}$, $R_s = 10^3$ with three different values of σ. The first three columns of values were obtained with $K = 6, 8, 10$ respectively for $\sigma = 1$ and are meant to show the accuracy of the representation. The next two columns were obtained with $\sigma = 10$ and $\sigma = 0\cdot1$ and show the dependence of Nu^s and Nu on σ. The last column gives the values of Nu for the case with $\sigma = 1\cdot0$, $R_s = 0$. As R becomes large the values of Nu for $\sigma = 1\cdot0$, $R_s = 10^3$ are seen to approach those with no stabilizing salt gradient ($R_s = 0$). The symbol Osc. means that the flow is oscillatory. Values of $1\cdot0$ correspond to no convection.

we observe that at $R = 2000$ and $R = 2500$ the results agree to four significant digits for $K = 8$ and $K = 10$ and at $R = 5000$ the value of Nu^s with $K = 10$ differs by $1\cdot5\%$ from that obtained with $K = 8$. At $R = 10{,}000$ the value for Nu^s with $K = 10$ differs so much (*ca.* 7%) from that with $K = 8$ that it is clear that the representation should be increased. Since we wish to consider results for Nu and Nu^s which are accurate to 1%, we shall restrict our attention to the range of R for which this accuracy is obtained. *All results reported in the remainder of this paper satisfy the criterion that the estimated error is less than 1%.*

Turning our attention now to the physical content of the results tabulated in table 1, we note first that the values for $\sigma = 1$, $K = 10$ show that the fluid exhibits oscillatory behaviour for $1797 \leqslant R < 2000$ and a well-developed, finite-amplitude steady motion at $R = 2000$. In view of the fact that the point of instability to overstable modes occurs at $R^o = 1797$ it is clear that the fluid first

becomes unstable to overstable motions and these persist, increasing in amplitude as R is increased. When R reaches a value between 1900 and 2000, finite-amplitude instability to a steady convective mode occurs and the system settles into a steady convective pattern. The amounts of heat and solute convected by the overstable modes are somewhat smaller than the amounts convected by steady modes. Hence, the basic thermal and solute fields are not distorted as much as they are when the steady convective mode is established.

An additional point which we note in this case is that the value of R^f obtained with $K > 2$ is considerably higher than that derived with $K = 2$. This has been found to be true in all of the calculations which have been carried out. The value of R^f is still substantially lower than R^c ($= 3820$). From this general behaviour we deduce that the minimum number of modes used for the representation in I grossly underestimates the minimum value of R at which finite-amplitude instability occurs.

The next two columns in table 1 list the values of Nu^s and Nu obtained with $K = 10$ for fluids with $\sigma = 0.1$ and $\sigma = 10$. It is evident that the dependence of Nu and Nu^s on Prandtl number is very weak, at least for the range shown, with differences of the order of 4 % or less. At $R = 1900$ calculations with $\sigma = 0.1$ show that the system simply decays, whereas for $\sigma = 1$ and $\sigma = 10$ the fluid exhibits oscillatory behaviour. This qualitative difference in behaviour can be directly traced to the linear stability analysis since $R^o = 3981$ for the case with $\sigma = 0.1$ and $R^o < 1900$ for the other two cases. Hence instability is first manifested as a finite-amplitude steady mode when $\sigma = 0.1$. We note also that the values of Nu and Nu^s for $\sigma = 1$ and $\sigma = 10$ are closer to each other than they are to those for $\sigma = 0.1$. This behaviour is presumably an extension of the qualitatively different response of the fluid with $\sigma = 0.1$ to infinitesimal perturbations. The values of Nu and Nu^s show a more uniform variation with σ when R is relatively large.

Although the presence of a stabilizing gradient of solute will serve to inhibit the onset of convection, the strong finite-amplitude motions which exist at sufficiently large Rayleigh numbers tend to mix the solute and distribute it so that the interior layers of the fluid are more nearly neutrally stratified. When this happens, the inhibiting effect of the solute gradient is greatly reduced and the fluid can convect nearly as much heat as it does in the absence of the solute. The column headed by $R_s = 0$ in table 1 gives the Nusselt number obtained when no solute is present and we see that as R increases the values of Nu with $R_s = 10^3$, $\sigma = 1$ approach the values with $R_s = 0$.

Calculations of Nu and Nu^s as functions of R for a range of R_s yield several important pieces of information. One is a corrected estimate of R^f, the minimum value of the Rayleigh number for which finite-amplitude steady motions occur. The analysis with $K = 2$ shows that R^f tends to τR_s as R_s becomes large. With a more complete representation of the T, S and ψ fields a better estimate is possible. In table 2 we list the numerical values of R^f obtained with $K = 2$ for a range of values of R_s and for fluids with $\sigma = 1, \tau = 10^{-\frac{1}{2}}$ and $\sigma = 1, \tau = 2^{-\frac{1}{2}}$. Also tabulated are ranges within which R^f lies according to the analysis with $K = 10$. For example, for $\sigma = 1$, $\tau = 10^{-\frac{1}{2}}$ at $R_s = 10^{\frac{5}{2}}$ no steady motion occurs with $R = 1200$

but a steady solution is obtained for $R = 1300$. Also given are the steady values of Nu and Nu^s for the larger of the two values of R in each entry (1300 in the example mentioned).

The above ranges for R^f ($K = 10$) for the fluid with $\sigma = 1$, $\tau = 10^{-\frac{1}{2}}$ are included as solid circles for the appropriate value of R_s in figure 1b.

R_s	R^f ($K = 2$)	R^f ($K = 10$)	Nu ($K = 10$)	Nu^s ($K = 10$)
		$\sigma = 1, \tau = 10^{-\frac{1}{2}}$		
$10^{\frac{5}{2}}$	1,178	1,200–1,300	1·714	3·219
10^3	1,773	1,900–2,000	1·787	3·307
$10^{\frac{7}{2}}$	3,130	4,100–4,200	2·355	4·163
10^4	6,490	10,600–10,700	3·086	5·381
		$\sigma = 1, \tau = 2^{-\frac{1}{2}}$		
$10^{\frac{5}{2}}$	None	None	None	None
10^3	2,000	2,000–2,100	1·369$_5$	1·632
$10^{\frac{7}{2}}$	4,280	4,400–4,500	2·208	2·668
10^4	10,450	11,300–11,400	2·590	3·080
2×10^4	18,780	21,300–21,400	2·964	3·505

TABLE 2. R^f *vs.* R_s for $\sigma = 1$. Values of R^f obtained with $K = 2$ are shown for several values of R_s for fluids with $\sigma = 1$, $\tau = 10^{-\frac{1}{2}}$ and $\sigma = 1$, $\tau = 2^{-\frac{1}{2}}$. Also tabulated are the ranges of R within which R^f occurs when $K = 10$. The values of Nu and Nu^s correspond to the larger value of R in each range.

We observe first that the values of R^f obtained with $K = 10$ are substantially higher than those obtained with $K = 2$. The most significant qualitative result which appears is that finite-amplitude motions occur only for values of R greater than R_s. In other words, the imposed temperature difference must at least compensate for the imposed solute difference for steady motion to exist. Although this result is available only for fluids with $\tau = 10^{-\frac{1}{2}}$ and $2^{-\frac{1}{2}}$ and the ranges of R_s which are shown, it is probably a general result. Certainly it has intuitive appeal, especially since $R^f/R_s \to 1$ as $R_s \to \infty$. The indications are that for large R_s, once the stability becomes even mildly superadiabatic, very strong convective motions are generated.

When convection occurs, more solute and heat will be transported than by conduction alone. Since the fluid layer is stably stratified by S and unstably stratified by T, positive buoyancy will be generated by the vertical flux of solute and negative buoyancy by the vertical flux of heat. The net result of these two processes will be a flux of density through the fluid.

We can derive an expression for the density flux through the fluid in the following way: the non-dimensional density perturbation is defined as

$$\delta\rho/\rho_m = \beta\delta S - \alpha\delta T = \beta\Delta S(-z+S) + \alpha\Delta T(z-T) \tag{4.5}$$

and the associated vertical density gradient is given by

$$\frac{\partial}{\partial z}\left(\frac{\delta\rho}{\rho_m}\right) = \beta\Delta S\left(-1+\frac{\partial S}{\partial z}\right) + \alpha\Delta T\left(1-\frac{\partial T}{\partial z}\right). \tag{4.6}$$

The non-dimensional density flux, F^ρ, at the boundary $z = 0$ can be written as

$$F^\rho = -\kappa_s \beta \Delta S \left(-1 + \frac{\partial S}{\partial z} \Big|_{z=0} \right) - \kappa \alpha \Delta T \left(1 - \frac{\partial T}{\partial z} \Big|_{z=0} \right)$$
$$= \kappa_s \beta \Delta S \, Nu^s - \kappa \alpha \Delta T \, Nu. \tag{4.7}$$

A convenient scaling is obtained by defining the density flux in units of the non-dimensional heat flux due to the imposed temperature difference, i.e.

$$\frac{F^\rho}{\kappa \alpha \Delta T} = \tau \frac{R_s}{R} Nu^s - Nu. \tag{4.8}$$

When the first term on the right-hand side exceeds the second, the density flux will be positive upward and vice versa. Hence, since we note from table 1 that the ratio Nu^s/Nu is approximately constant (somewhat less than 2), the downward density flux increases as R increases.

On the other hand, consider the value of the density flux as a function of R_s when steady motions can just be established, i.e. at $R = R^f$. We noted earlier that R^f/R_s starts off with a value larger than unity for small R_s and approaches unity as R_s becomes large. Hence, for small values of R_s, the first term in (4.8) will be relatively smaller and the density flux will be more negative. As $R_s \to \infty$, $R_s/R^f \to 1$ and the first term becomes larger. From table 2 we can substitute the pertinent numbers and we find that for the cases with $\tau = 10^{-\frac{1}{2}}$ and $\tau = 2^{-\frac{1}{2}}$ the first term in (4.8) approaches a limit given by

$$\tau \frac{R_s}{R} Nu^s \to \tau^{\frac{1}{2}} Nu \quad \text{as} \quad \frac{R_s}{R^f} \to 1. \tag{4.9}$$

If we now define a diffusion coefficient for density, κ_ρ, by dividing (4.7) by the negative of (4.6) evaluated at the boundary, we find

$$\kappa_\rho \equiv \frac{F^\rho}{-\partial/\partial z \, (\delta\rho/\rho_m)_{z=0}} = \frac{\kappa_s R_s Nu^s - \kappa R \, Nu}{R_s \, Nu^s - R \, Nu} = \kappa \frac{\tau R_s Nu^s - R \, Nu}{R_s \, Nu^s - R \, Nu}, \tag{4.10}$$

and substituting (4.9) yields

$$\kappa_\rho \to \frac{\kappa(\tau^{\frac{1}{2}} - 1) R \, Nu}{(\tau^{-\frac{1}{2}} - 1) R \, Nu}$$

or
$$\kappa_\rho \to -(\kappa\kappa_s)^{\frac{1}{2}}. \tag{4.11}$$

Hence, the density will 'diffuse' with a negative molecular diffusion coefficient whose magnitude is the square root of the product of the two diffusivities. It is not clear how the idea of such a negative diffusion coefficient will be useful but the above result seems to be a general one for the steady flows. The reason for the negative diffusion coefficient is clear. The solute gradient at the boundary must be considerably sharper than the temperature gradient and the net effect on the density is to create a stable density field. Yet the convecting fluid must be transporting negative density upward. Hence, the flow of density is up the gradient.

I mentioned the above result to Dr Claes Rooth, who subsequently produced an alternative derivation of (4.11). In his argument he assumes that boundary

layers of solute and temperature are formed near $z = 0$ and that the fluxes can be expressed as diffusive fluxes in terms of the imposed quantities ΔT and ΔS and the boundary-layer scales l_s and l_h. Thus, denoting the respective contributions of heat flux and solute flux to the density flux by HF and SF respectively, he has

$$HF = -\frac{\kappa\alpha\Delta T}{l_n}, \quad SF = \frac{\kappa_s\beta\Delta S}{l_s}$$

and the ratio in the limit of $R_s/R^f \to 1$ ($\alpha\Delta T/\beta\Delta S \to 1$) is

$$HF/SF \to -\kappa l_s/\kappa_s l_n.$$

Rooth takes the diffusive scales to be proportional to the square root of the diffusion; then

$$l_s/l_n \approx (\kappa_s/\kappa)^{\frac{1}{2}}$$

and

$$HF/SF \to -\tau^{-\frac{1}{2}}.$$

This statement is equivalent to our (4.9) and the rest of the argument follows that given above.

Solute and temperature distributions

More detailed information about the behaviour of the convecting fluid may be obtained from the spatial distributions of the temperature, solute and density fields. We shall show contours of S and T as defined by the non-dimensional quantities,

$$\frac{T_{\text{total}} - T_m}{\Delta T} \quad \text{and} \quad \frac{S_{\text{total}} - S_m}{\Delta S}.$$

The perturbation density field is given by (4.5). On multiplying (4.5) by $gd^3/\kappa\nu$ we can define a non-dimensional density as

$$\frac{g(\delta\rho/\rho_m)d^3}{\kappa\nu} = R_s(-z+S) + R(z-T). \tag{4.12}$$

Finally, to normalize the above expression we write

$$\rho \equiv \frac{\delta\rho/\rho_m}{\alpha\Delta T} = z - T + \frac{R_s}{R}(-z+S). \tag{4.13}$$

Equation (4.13) defines the density perturbation in units of the density difference associated with the imposed difference in temperature, ΔT, across the fluid layer.

Figures $2a$, $2b$ and $2c$ show contours of T, S and ρ in a half-cell for the case $\sigma = 1, \tau = 10^{-\frac{1}{2}}, R_s = 10^3, R = 2500$. Convection is fairly strong (the corresponding Nusselt number is 2·505) and the formation of anvil-shaped plumes of isotherms is just noticeable in figure $2a$. Such plumes are characteristic of strong cellular motions in Bénard convection and have also been derived for convection in a rotating system when the rotation is not too strong (Veronis 1968). The isotherms in the centre of the cell are more or less vertical and become horizontal near the upper and lower boundaries where conduction is important. Also, since conditions of symmetry at the lateral sides of the cell require that $\partial T/\partial x = 0$ there, the isotherms are flat near $x = 0$ and $x = 1/\alpha$.

The contour pattern for the solute shows a more homogeneous structure near the centre of the cell (figure 2*b*). The fluid is much more thoroughly mixed and a large region near the centre has a solute concentration of about $S = 0.5$. The
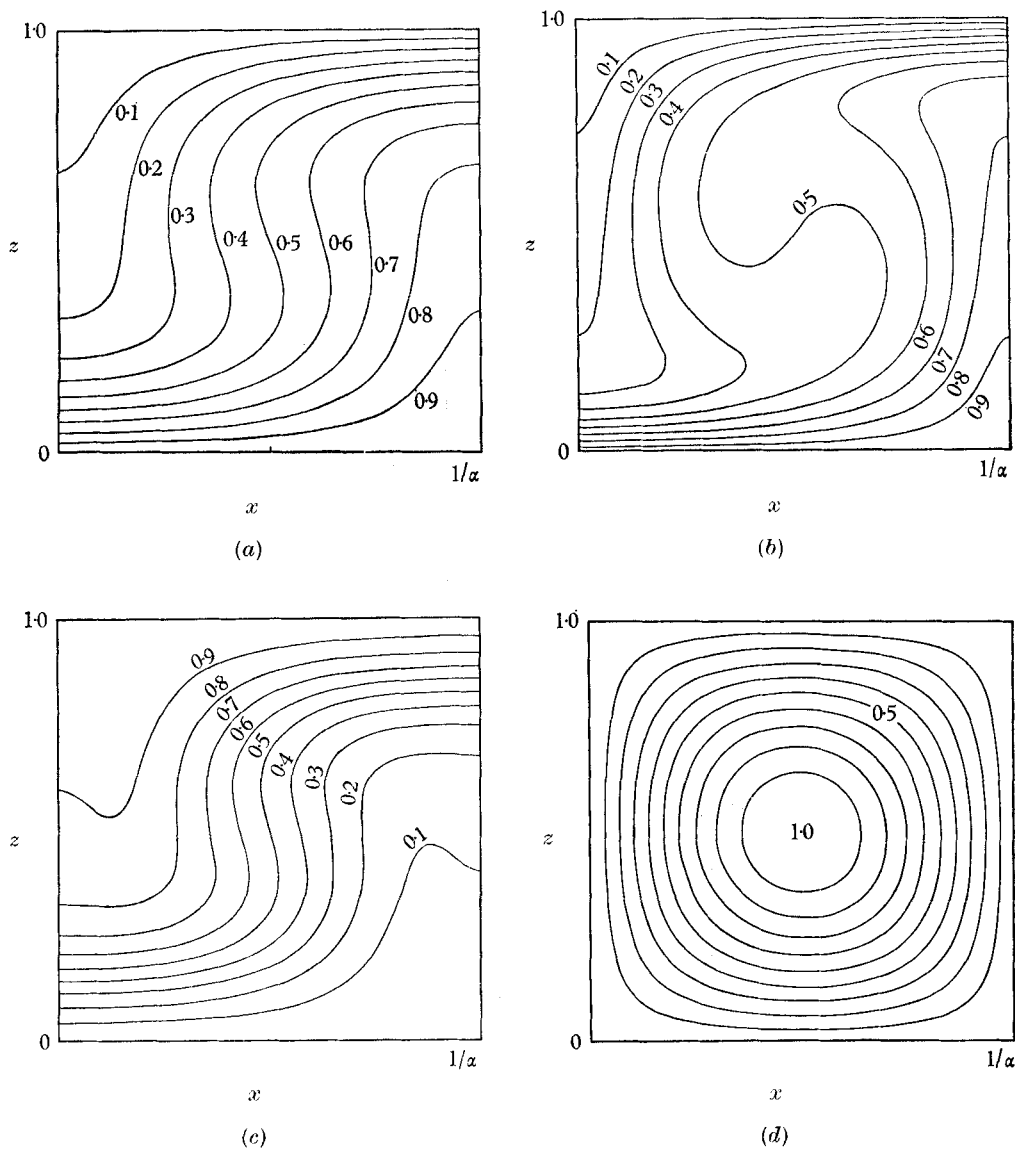
FIGURE 2. Contour lines of (*a*) T, (*b*) S, (*c*) ρ and (*d*) ψ in a half-cell. The lines $x = 0$ and $x = 1/\alpha$ are lines of symmetry for T, S and ρ and lines of antisymmetry for ψ. For this case $\tau = 10^{-\frac{1}{2}}$, $\sigma = 1$, $R_s = 10$, $R = 2500$.

vertical contour lines extend closer to the lateral boundaries than do the iso-therms and the boundary layers near the edges of the cell are thinner. This structure simply reflects the fact that κ_s is less than κ so that a sharper boundary gradient for S is necessary to support flux of solute into or out of the fluid. Also,

when convective motion has mixed the fluid, the process of diffusion of the solute concentration (which tends to establish the linear distribution of S in the vertical to comply with the boundary values) is less effective and the fluid is more homogeneous near the centre.

The density distribution in figure 2c reflects the structure of the temperature in the interior of the cell where S is more nearly uniform. The gradient of the density near the upper and lower boundaries is smaller than that of either S or T because the density contains the opposing effect of these two gradients. The range of ρ is 0·6 non-dimensional units and is discussed below in connexion with figure 3c.
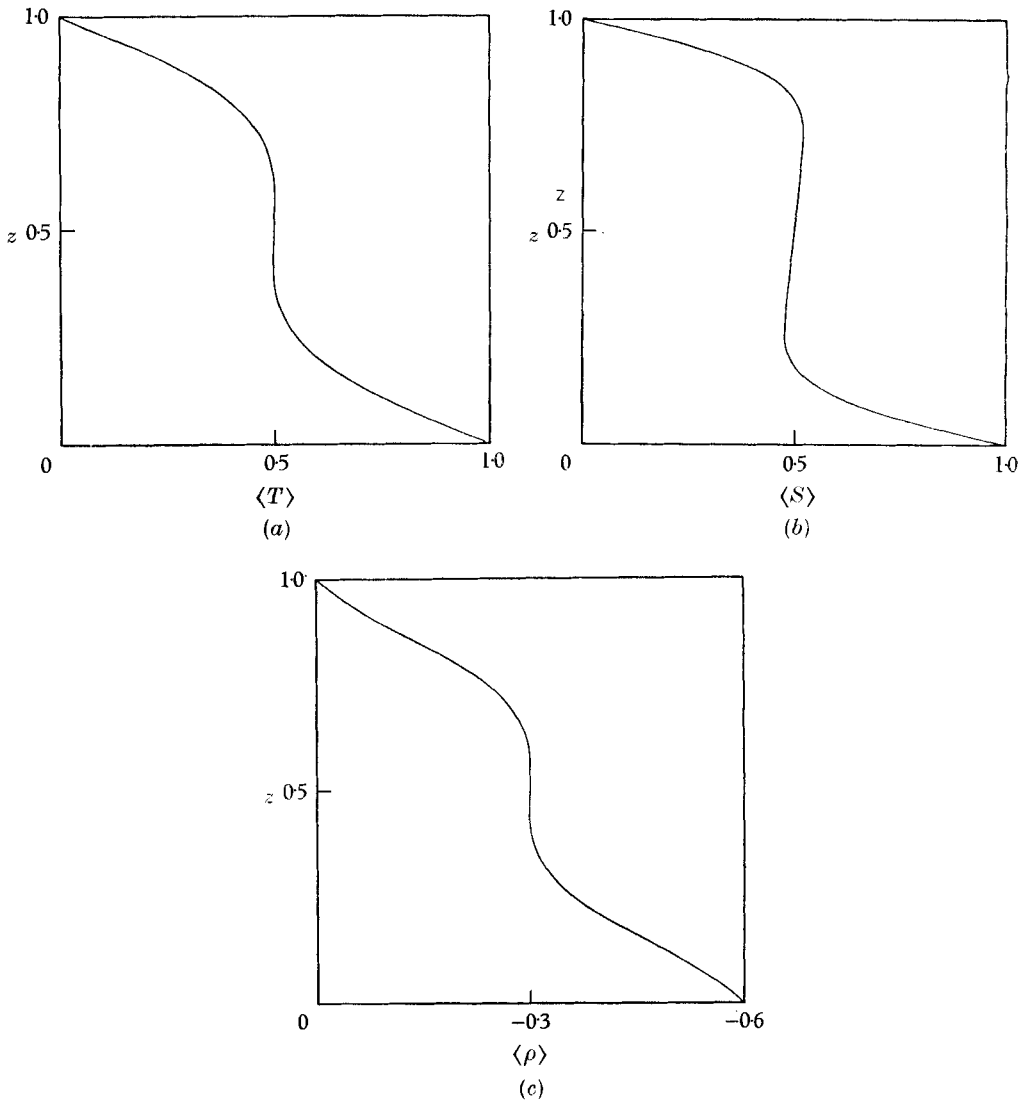
FIGURE 3. Graphs of (*a*) $\langle T \rangle$, (*b*) $\langle S \rangle$ and (*c*) $\langle \rho \rangle$ as functions of the vertical co-ordinate, z, for the same values of τ, σ, R_s and R as in figure 2.

Figure 2*d* shows the streamline pattern for the flow. This structure is character-istic of all of the two-dimensional convective motions which have been derived, with or without rotation or a solute concentration.

Figures 3*a*, 3*b* and 3*c* show the horizontally averaged temperature, $\langle T \rangle$, solute, $\langle S \rangle$, and density, $\langle \rho \rangle$, distributions as functions of the vertical co-ordinate z. The temperature, $\langle T \rangle$, exhibits a nearly isothermal structure near the centre of the cell and, in fact, the vertical temperature gradient is very slightly positive in the middle. The solute, $\langle S \rangle$, shows a stronger boundary-layer structure with an obvious reversal in the mid-region of the cell. This reversal of the gradients of the horizontally averaged quantities has been deduced for temperature in previous studies of two-dimensional Bénard convection.

The vertically averaged density field again exhibits the opposing effects of temperature and salinity and we remark that boundary gradients are smaller and so is the region of nearly zero gradient in the middle. Observe, also, that the range of the density variation is 0·6 non-dimensional units. This range is due to the fact that the 1·0 amount of destabilizing temperature at $R = 2500$ is offset by 0·4 units of stabilizing solute ($R_s = 1000$).

Similar pictures of steady fields have been constructed for both larger and smaller values of R. The qualitative behaviour is the same with more (less) uniform distribution of S in the mid-regions for larger (smaller) R.

5. Oscillatory motions of large amplitude

All of the calculations with $\sigma \geqslant 1$ show that the first instability is an infinitesi-mal oscillatory motion. A subcritical finite-amplitude oscillatory motion was not observed in any of the runs. For R in the range $R^o < R < R^f$ a finite-amplitude oscillatory motion is established. We know from the analysis of convection in a rotating system that when steady motions finally do occur there is a jump in the value of the heat transport over that due to overstable motions. The same general property has been observed in the present system. Some specific results from the calculations for oscillating motions are discussed here.

Table 3 summarizes the information about the periods of the finite-amplitude oscillations for four cases—one with $R_s = 10^3$, one with $R_s = 10^4$ and two with $R_s = 10^{\frac{7}{2}}$. Listed for each case are the period at the point of instability, $R = R^o$, and the period at some value $R > R^o$. The oscillatory motions which occur for $R > R^o$ are no longer simple harmonic motions since there is considerable dis-tortion of the sinusoidal forms which exist at the point of instability. Hence, the calculations were extended until the field variables exhibited cyclic (albeit not simple harmonic) behaviour and the period is the time taken for a cycle. It is evident that finite amplitude serves to increase the period of the oscillations in the four cases. This was found to be true in all of the calculations which were made of finite-amplitude oscillatory motions.

Figure 4 gives a more detailed picture of the oscillations for the case with $\sigma = 1$, $\tau = 10^{-\frac{1}{2}}$, $R_s = 10^{\frac{7}{2}}$, $R = 4000$. The system has settled into a cyclic response and several integral properties are shown as functions of time, starting from an arbitrary point in the cycle. Nu and Nu^s are again measures of the flux of heat

and solute respectively through the bottom boundary and $F^\rho/\kappa\alpha\Delta T$ is the density flux defined in (4.9). Since the fluid is being heated from below, the net density flux upward will be negative and, with the foregoing definition, $-F^\rho/\kappa\alpha\Delta T$ will be positive. The units of Nu, Nu^s and $-F^\rho/\kappa\alpha\Delta T$ are shown on the left-hand ordinate. The right-hand ordinate marks the units for ψ_{max}, the maximum value

R_s	R^o	Period at R^o	R	Period at R
10^3	1,797	0·654	1,900	0·708
$10^{\frac{7}{2}}$	3,220	0·341	3,500	0·367
$10^{\frac{7}{2}}$	3,220	0·341	4,000	0·467
10^4	7,220	0·188	8,800	0·227

TABLE 3. Periods of oscillatory motions for $\tau = 10^{-\frac{1}{2}}$, $\sigma = 1$. The periods of the oscillatory motions are listed in the third and fifth columns respectively for $R = R^o$ and for a value of $R > R^o$
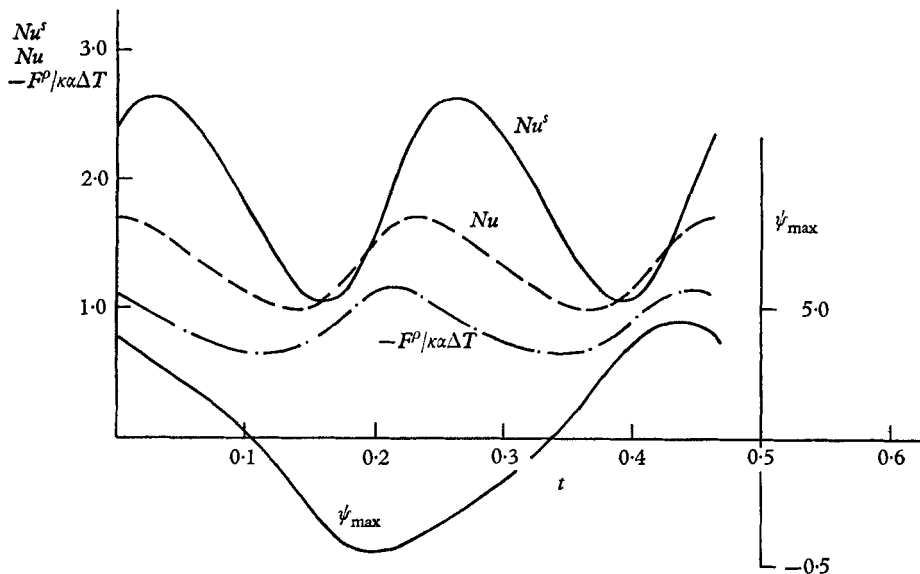
FIGURE 4. The quantities Nu, Nu^s, $-F^\rho/\kappa\Delta T$ and ψ_{max} are shown as functions of time for one cycle of oscillation of the basic variables for the case $R_s = 10^{\frac{7}{2}}$, $\tau = 10^{-\frac{1}{2}}$, $\sigma = 1$, $R = 4000$. Since Nu, Nu^s and $-F^\rho/\kappa\alpha\Delta T$ are derived quantities which depend on non-linear interactions of the basic variables, they execute two complete oscillations during one period. The origin is chosen (arbitrarily) as $t = 0$ and the length of the period is approximately 0·45 non-dimensional units.

of the streamfunction, which is also plotted. Since $\psi = 0$ on the boundaries of the half-cell, the value of ψ_{max} is a measure of the intensity of the circulation.

The period for Nu, Nu^s and $-F^\rho/\kappa\alpha\Delta T$ is half that of ψ_{max}. The reason for this is that the oscillatory behaviour of the fluxes arises from the covariance of the velocity and fluctuating temperature or salinity. If ψ and T each have a given period of oscillation, the covariance will yield the half period.

The quantity $-F^\rho/\kappa\alpha\Delta T$ has the value 0·75 when the fluid is conducting. We see from the figure that during most of the cycle the density flux exceeds the value
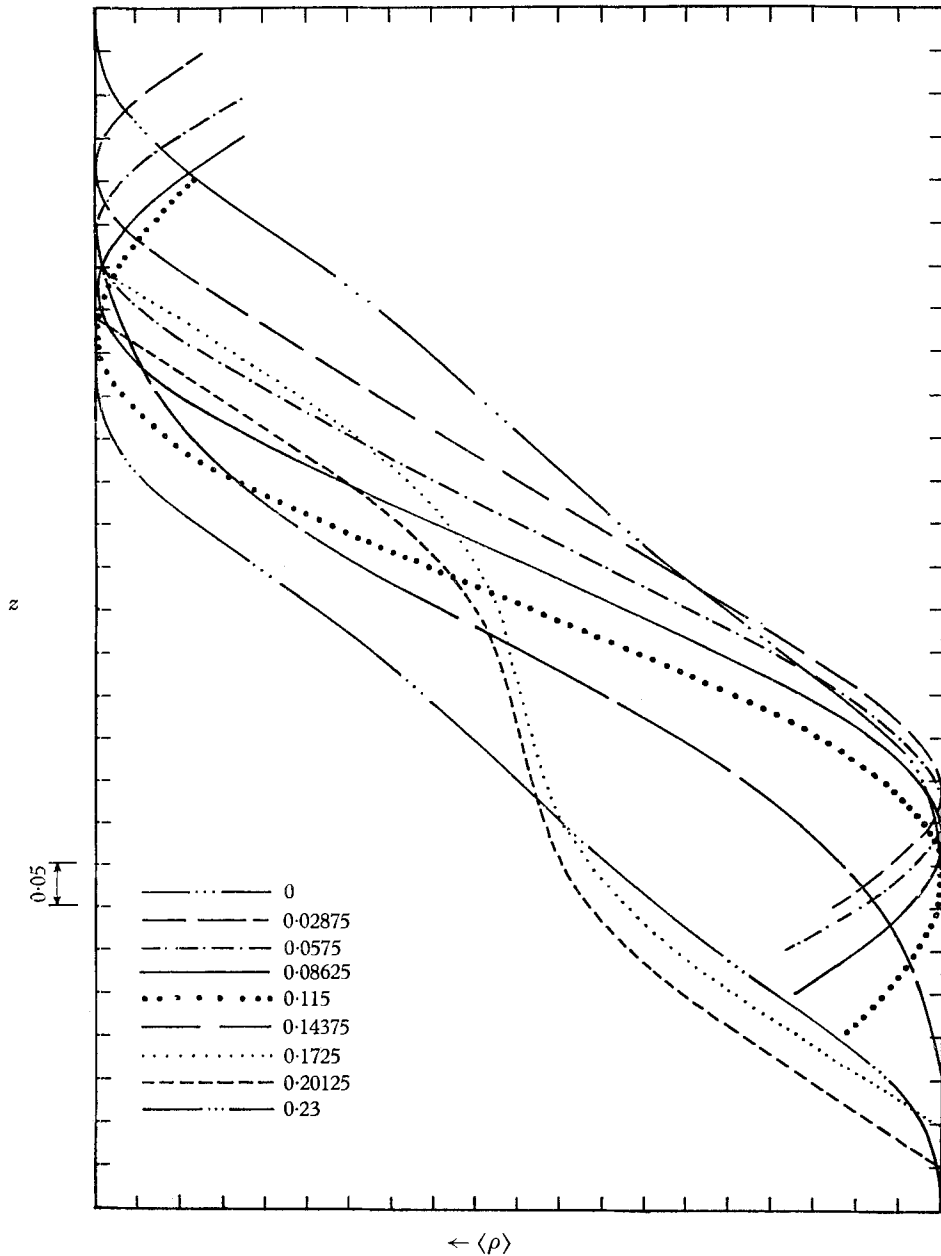
FIGURE 5. Vertical profiles of horizontally averaged density, $\langle \rho \rangle$, are shown at nine times during the half cycle, $0 \leqslant t \leqslant 0.23$, of figure 4. The time of each profile is listed in the legend on the lower left. The abscissa axis for each successive profile is displaced downward one unit (each unit equals 0·05). The range of $\langle \rho \rangle$ from endpoint to endpoint of each curve is the same. The range of variation for $\langle \rho \rangle$ for the curve at $t = 0.0575$, for example, is about 30% greater than the range of $\langle \rho \rangle$ at $t = 0$. Therefore the curves in the range $0.02875 \leqslant t \leqslant 0.115$ have a total range of $\langle \rho \rangle$ greater than the range imposed by the boundary conditions.

0·75. This excess flux due to convection is a familiar behaviour encountered in all problems of this type. For a part of the cycle, however, the density flux is less than that due to conduction. Since the density flux is a function of τ as well as Nu and Nu^s and since Nu and Nu^s are not in phase, there are time intervals in each cycle during which the density fluxes due to Nu and Nu^s tend to cancel each other more than they do for conduction alone. During these periods the net density flux is small.

When the net density flux is smaller than that due to conduction alone, the convective process must create a sharper gradient of solute near the boundaries so that the flux of solute into the layer, measured in terms of the effect on density, yields a more stable gradient near the boundaries. Since the temperature and solute fields are out of phase, the structure of the density field during a cycle is not *a priori* obvious. To provide a clearer picture we show in figure 5 a sequence of vertical profiles of the horizontally averaged density field for nine equally spaced times in a cycle of the density flux, i.e. beginning at $t = 0$ in figure 4 and ending with $t = 0·23$. These profiles show that, during part of the cycle, layers of gravitationally stable fluid are present in the boundary regions and a strongly unstable layer exists in the mid-regions of the layer. For the remaining interval the fluid has unstable gradients near the boundaries with a more neutrally stable density distribution in the interior.

During that portion of the cycle in which the density gradient is stable near the boundaries $z = 0$ and $z = 1$, the density within the fluid has a value lying outside of the range of the imposed density distribution. The solute and temperature distributions still lie within the imposed ranges but relative changes of these quantities give rise to what seems at first to be anomalous density behaviour. It is clear that the possible range of density variation cannot exceed the values determined by the effects of solute and temperature acting individually.

REFERENCES

SANI, R. L. 1965 On finite amplitude roll-cell disturbances in a fluid subjected to a heat and mass transfer. *Am. Inst. Chem. Eng. J.* **11**, 971–980.

TURNER, J. S. 1965 The coupled turbulent transports of salt and heat across a sharp density interface. *Int. J. Heat Mass Transfer*, **8**, 759–767.

TURNER, J. S. 1968 The behaviour of a stable salinity gradient when it is heated from below (preprint).

TURNER, J. S. & STOMMEL, H. 1964 A new case of convection in the presence of combined vertical salinity and temperature gradients. *Proc. U.S. Nat. Acad. Sci.* **52**, 49–53.

VERONIS, G. 1965 On finite amplitude instability in thermohaline convection. *J. Mar. Res.* **23**, 1–17.

VERONIS, G. 1966 Large-amplitude Bénard convection. *J. Fluid Mech.* **26**, 49–68.

VERONIS, G. 1968 Large-amplitude Bénard convection in a rotating fluid. *J. Fluid Mech.* **31**, 113–140.